

Isometric immersions, energy minimization and self-similar buckling in non-Euclidean elastic sheets.

JOHN GEMMER¹, ERAN SHARON², TOBY SHEARMAN³ and SHANKAR C. VENKATARAMANI^{3,4}

¹ Division of Applied Mathematics, Brown University, Providence, RI 02906, USA

² Racah Institute of Physics, The Hebrew University, Jerusalem, 91904, Israel

³ Program in Applied Mathematics, University of Arizona, Tucson, AZ 85721, USA

⁴ Department of Mathematics, University of Arizona, Tucson, AZ 85721, USA

PACS 89.75.Kd – Patterns
 PACS 87.10.Pq – Elasticity theory
 PACS 02.40.-k – Geometry, differential geometry, and topology

Abstract – The edges of torn plastic sheets and growing leaves often display hierarchical buckling patterns. We show that this complex morphology (i) emerges even in zero strain configurations; (ii) is driven by a competition between the two principal curvatures, rather than between bending and stretching. We identify the key role of branch-point (or “monkey-saddle”) singularities in generating complex wrinkling patterns in isometric immersions, and show how they arise naturally from minimizing the elastic energy.

arXiv:1601.06863v1 [cond-mat.soft] 26 Jan 2016

Introduction. – The rippling patterns observed in torn plastic sheets [1–3], leaves [4–8] and swelling hydrogels [9–11] provide striking examples of periodic and self-similar patterns; see fig. 1. Within the formalism of finite elasticity, such patterns are understood as resulting from the sheet buckling to relieve growth induced residual strains [12, 13]. On the one hand, complex, self-similar patterns in elastic sheets can arise from boundary conditions that preclude the possibility of relieving in-plane strains [14–16]. On the other hand many growth patterns generate residual in-plane strains which can be entirely relieved by the sheet forming an isometric immersion of a hyperbolic Riemannian metric; indeed smooth hyperbolic metrics on bounded domains can always be immersed in \mathbb{R}^3 by smooth isometries [17] (but not so for unbounded domains [18–20]). Why then do we observe self-similar buckling patterns in free elastic sheets? In this letter we report on multiple strands of recent work, that, taken together, address this puzzle.

We show that a large class of growth profiles admit smooth (*i.e.* infinitely differentiable) as well as (many) non-smooth configurations of the sheet with vanishing in-plane strain. The non-smooth configurations are piecewise surfaces constructed by gluing together isometries along “lines of inflection” and at “branch points” in such a manner that the resulting surface does not concentrate bending energy. We also show that minimizing the bending energy among the various isometric immersions naturally leads to complex, self-similar, wrinkling patterns. These patterns arise from a competition between the energetic contributions of the two principal curvatures in an isometric im-

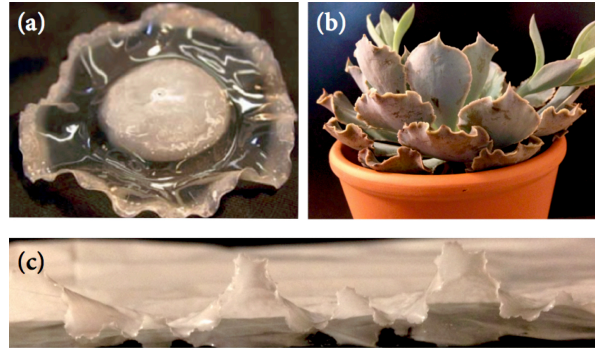


Fig. 1: Examples of complex wrinkling patterns in swelling thin elastic sheets. (a) Hydrogel disk with non-uniform swelling pattern. (b) Ornamental echeveria house plant. (c) Edge of a torn trash bag.

ersion. This mechanism is in contrast to earlier explanations [2] which argued that the self-similar profiles result from a balance between the stretching and bending energies. Finally, we show that, the widely used Föppl-von Kármán approximation for thin elastic sheets can, in certain circumstances, give results that differ significantly from a full nonlinear elastic model.

The non-Euclidean formalism of thin sheet elasticity [21] posits that growth permanently deforms the intrinsic distance between material points, so growth is encoded in a Riemannian metric \mathbf{g} . Specifically, material points on the center surface are labelled by coordinates $(x, y) \in \Omega$, a subset of \mathbb{R}^2 , and the dis-

tance between such points is given by the arc-length element:

$$ds^2 = g_{11}(x, y)dx^2 + 2g_{12}(x, y)dxdy + g_{22}(x, y)dy^2.$$

By the Kirchhoff hypothesis [22], the conformation of the sheet as a 3-dimensional object in \mathbb{R}^3 is determined by an immersion $F : \Omega \rightarrow \mathbb{R}^3$ of the center surface. The equilibrium configuration is then taken to be a global minimizer of an elastic energy modeled as the sum of stretching and bending contributions:

$$\begin{aligned} E[F] &= \mathcal{S}[\gamma] + t^2 \mathcal{B}[H, K] \\ &= \int_{\Omega} Q(\gamma) dxdy + t^2 \int_{\Omega} (4H^2 - 2K) dxdy, \end{aligned} \quad (1)$$

where $\gamma = (\nabla F)^T \cdot \nabla F - \mathbf{g}$ denotes the in-plane strains in the center surface, t is the thickness of the sheet, Q is a quadratic form, and H and K are respectively the mean and Gaussian curvatures of the center surface [21, 23]. The $t \rightarrow 0$ (vanishing thickness) limits of minimizers of the elastic energy (1) are necessarily $W^{2,2}$ isometric immersions $F : (\Omega, \mathbf{g}) \rightarrow \mathbb{R}^3$ [24].

Rather than use the (technical) notion of $W^{2,2}$ isometric immersions, we define (piecewise smooth) isometries with finite bending content as configurations F satisfying (i) ∇F is continuous; (ii) $(\nabla F)^T \cdot \nabla F = \mathbf{g}$; (iii) $D^2 F$, the Hessian of F , is piecewise smooth; and (iv) $\int_{\Omega} (4H^2 - 2K) dxdy < \infty$.

Such configurations are indeed $W^{2,2}$ isometries. To illustrate the physical import of our definition, we note that the vanishing thickness limits of elastic ridges [25] and d -cones [26] violate condition (i). They are neither in this class, nor in $W^{2,2}$; indeed the bending content of these defects diverges as $t \rightarrow 0$.

Power law metrics and single wavelength isometries. – Motivated by the preceding discussion, we investigate isometric immersions of the strip $\Omega = \mathbb{R} \times [0, W]$ with the metric

$$\mathbf{g} = (1 + 2\epsilon^2 f(y)) dx^2 + dy^2, \quad f(y) = \frac{\alpha}{4(\alpha + 1)} \left(1 + \frac{y}{l}\right)^{-\alpha} \quad (2)$$

where $\alpha \in (0, \infty)$, l is a length scale and $\epsilon > 0$. This metric corresponds to y dependent growth in the x direction localized near the $y = 0$ edge of the sheet and includes the metrics considered in [2, 3, 6, 8, 16] as particular cases. For $\epsilon \ll 1$, approximate isometries are obtained from the Föppl - von Kármán ansatz $F(x, y) = (x + \epsilon^2 u^0, y + \epsilon^2 v^0, \epsilon w^0)$ with $O(\epsilon^2)$ in-plane and $O(\epsilon)$ out-of-plane deformations. In this small slope geometry, *i.e.* for $\epsilon \ll 1$, the mean and Gaussian curvatures are given by $H = \frac{\epsilon}{2} \Delta w^0$ and $K = \epsilon^2 \det(D^2 w^0)$ [27]. If $w = w^0$ satisfies

$$\det(D^2 w(x, y)) = -f''(y) = -\frac{\alpha^2}{4} \left(1 + \frac{y}{l}\right)^{-\alpha-2}, \quad (3)$$

the small-slope version of Gauss' Theorema Egregium, we can solve for u^0 and v^0 to obtain isometries at $O(\epsilon^2)$ [27]. We seek product solutions of eq. (3) in the form $w^0(x, y) = \psi(x)\phi(y)$, $\phi(y) = (1 + y/l)^{-\alpha/2}$. Then ψ satisfies $\psi'(x)^2 - \delta^{-1} \psi''(x)\psi(x) = 1$ with first integral

$$\psi'^2 \pm k^{2\delta} |\psi|^{2\delta} = 1, \quad (4)$$

where $\delta = \alpha/(2 + \alpha)$, $k > 0$ and $\pm k^{2\delta}$ is a constant of integration. We can identify periodic solutions $\psi(x)$ with the motion of a unit mass particle in the potential $V(\psi) = +\frac{1}{2}(k|\psi|)^{2\delta}$.

Let $\psi_1(x)$ be given by $\psi_1'^2 + |\psi_1|^{2\delta} = 1$, $\psi_1(x) > 0$ on $(-\lambda_1, \lambda_1)$ and $\psi_1(\pm\lambda_1) = 0$. Then $\lambda_1(\delta) = \int_0^1 (1 - s^{2\delta})^{-1/2} ds$. Defining $\psi_k(x) = k^{-1} \psi_1(kx)$ yields a solution of eq. (4) with quarter-wavelength $\lambda_k = \lambda_1/k$. The product solution of (3) given by $w^0(x, y) = \psi_k(x)(1 + y/l)^{-\alpha/2}$ has mean curvature

$$H(x, y) = \frac{\epsilon}{2} \Delta w^0 = \epsilon \left[\frac{c_1(\xi)}{k l^2 (1 + y/l)^{\alpha/2+2}} - \frac{c_2(\xi)k}{(1 + y/l)^{\alpha/2}} \right],$$

where $\xi = kx$, and $c_{1,2}$ are positive functions, independent of k .

$$\eta \equiv \frac{H}{\sqrt{|K|}} = \frac{1}{2} \left(\sqrt{\frac{\kappa_1}{\kappa_2}} - \sqrt{\frac{\kappa_2}{\kappa_1}} \right) = \frac{1}{2} \left(\frac{c_0(\xi)kl}{(1 + y/l)} - \frac{(1 + y/l)}{c_0(\xi)kl} \right)$$

defines the *disparity* η where $\kappa_{1,2}$ are the *principal curvatures*.

Averaging $\epsilon^{-2} H^2$ over a quarter-period λ_k , we have the k dependence of \bar{B} , the normalized (by ϵ^2), nondimensional, bending content per unit length in the x direction:

$$\bar{B} \sim C_1 k^2 l \int_0^W \frac{dy}{(1 + y/l)^\alpha} + \frac{C_2}{k^2 l^3} \int_0^W \frac{dy}{(1 + y/l)^{\alpha+4}}$$

with C_1, C_2 positive constants. Let k^* denote the value of k that minimizes \bar{B} ; the optimal ‘‘global’’ wavelength λ_{glob} is given by:

$$\lambda_{glob} \sim \frac{\lambda_1}{k^*} \sim l \left| \frac{(1 + W/l)^{1-\alpha} - 1}{(1 + W/l)^{-3-\alpha} - 1} \right|^{\frac{1}{4}},$$

where we are taking $|(1 + W/l)^{1-\alpha} - 1| = \ln(1 + W/l)$ for $\alpha = 1$. We can also determine the optimal ‘‘local’’ wavelength $\lambda_{loc}(\zeta)$ by minimizing $\lambda_k^{-1} \int_0^{\lambda_k} H^2(x, \zeta) dx$ to obtain

$$\lambda_{loc}(\zeta) \sim l(1 + \zeta/l) = (\zeta + l).$$

This is related to the buckling wavelength for a thin strip cut out of the sheet [3, 8] near $y = \zeta$. $\lambda_{loc}(0) \approx \lambda_{glob}$, but for $W \gg l$, there is a range of y where $\lambda_{loc}(y)$ differs substantially from λ_{glob} , giving an energetic impetus for the sheet to increase the buckling wavelength as one moves away from the edge at $y = 0$.

There is, however, an obstruction to changing the wavelength in y . Let w denote an arbitrary solution of (3), and define the (non-vanishing) vector field $\mathbf{v}(x, y) = -\frac{w_{xy} w_{yy}}{2f''(y)} \mathbf{i} + \mathbf{j}$. The integral curves of \mathbf{v} foliate the strip Ω and are transversal to the curves $y = \text{const}$. A direct computation invoking the translation invariance (*i.e.* x -derivative) of (3) yields

$$\begin{aligned} \mathbf{v} \cdot \nabla (w_{xx}) &= -\frac{w_{xy} w_{yy} w_{xxx}}{2f''(y)} + w_{xxy} \\ &= \frac{w_{xy} w_{xyy} - w_{yy} w_{xxy}}{2f''(y)} w_{xx} \propto w_{xx}. \end{aligned} \quad (5)$$

This implies the curves along which $w_{xx} = 0$ cannot bifurcate, and thus the number of locations where $w_{xx} = 0$, and equivalently, the number of waves in the buckling patterns cannot change with y . How do we reconcile these mathematical results, *viz.* (i) there are strain free configurations of the sheet; and (ii) the smooth strain-free configurations are single wavelength; with the observed complex wrinkling patterns? The resolution is that, in obtaining eq. (5), we have implicitly assumed that w is thrice continuously differentiable; this is not necessarily true for surfaces with finite bending content.

Branch points in isometric immersions. – We define *lines of inflection* and *branch points* by first considering solutions of $\det(D^2w) = -1$. Let (x, y) and (r, θ) denote Cartesian and polar coordinates on \mathbb{R}^2 . The piecewise quadratic function

$$w(x, y) = ax + by + c + \begin{cases} y(x - y \cot(\theta_+)) & 0 \leq \theta \leq \theta_+ \\ y(x + y \cot(\theta_-)) & -\theta_- \leq \theta \leq 0 \end{cases}$$

with $0 < \theta_{\pm} < \pi$ is a solution to $\det(D^2w) = -1$ on the sector $S = \{-\theta_- \leq \theta \leq \theta_+\}$. The ray $\{\theta = 0\}$ is a *line of inflection* [28] if $\cot(\theta_+) \neq -\cot(\theta_-)$ – a principal curvature for the surface $z = w(x, y)$ is discontinuous across this line. The surface has a Lipschitz continuous [29] tangent plane everywhere on S , in particular across the line of inflection. The rays $\theta \in \{-\theta_-, 0, \theta_+\}$ all map into straight lines that lie in a common plane – the tangent plane to the surface at $(0, 0, c)$.

Given $2n$ (an even number), a sequence of angles $\theta_0 < \theta_1 < \theta_2 < \dots < \theta_{2n} = 2\pi + \theta_0$, and a plane (not parallel to the z -axis) $z = ax + by + c$, we can extend the above construction to define a piecewise quadratic function on \mathbb{R}^2 , where the angles θ_i define the lines of inflection by $x = x_0 + \cos(\theta_i)\lambda$, $y = y_0 + \sin(\theta_i)\lambda$, and $z = ax + by + c$, with $(x_0, y_0) \in \mathbb{R}^2$, $\lambda \geq 0$. This generalizes our construction in ref. [28] ($x_0 = y_0 = a = b = c = 0$, $\theta_i = \frac{2\pi i}{n}$).

The surface is smooth only if $n = 2$, $\theta_2 = \theta_0 + \pi$ and $\theta_3 = \theta_1 + \pi$. In particular, the surface is not smooth if $n \geq 3$. We then refer to the point (x_0, y_0) where the 6 or more lines of inflection meet as a *branch point* or *n-saddle*; (x_0, y_0) is indeed a branch point for the map $(x, y) \mapsto \nabla w$. In the sector $\theta_{i-1} \leq \theta \leq \theta_i$ we have $H = \eta = \pm \cot(\theta_i - \theta_{i-1})$. The principal curvatures are discontinuous across lines of inflection, but they are bounded: $\kappa_1^2 + \kappa_2^2 = 4H^2 + 2|K| \leq 2 + 4 \max_{i=1,2,\dots,2n} \cot^2(\theta_i - \theta_{i-1})$.

This construction allows us to introduce a branch point at *any given location* (x_0, y_0) in a (locally) quadratic surface satisfying $\det(D^2w) = -1$. The tangent plane at $(x_0, y_0, w(x_0, y_0))$ intersects the surface along 4 rays with azimuthal angles $\varphi_0, \varphi_1, \varphi_2 = \varphi_0 + \pi, \varphi_3 = \varphi_1 + \pi$. We can introduce a branch point at (x_0, y_0) using the tangent plane as the common plane, and defining a *daughter sequence* of angles $\theta_0 = \varphi_0 < \theta_1 < \theta_2 < \theta_3 = \varphi_1 < \theta_4 = \varphi_2 < \theta_5 = \varphi_3 < \theta_0 + 2\pi$. The sequence $\{0, \frac{3\pi}{4}, \pi, \frac{7\pi}{4}, 2\pi\}$ is unique in that all the sectors have disparity $\eta = \pm 1$ and the daughter sequence $\{0, \frac{\pi}{4}, \frac{\pi}{2}, \frac{3\pi}{4}, \pi, \frac{7\pi}{4}, 2\pi\}$ corresponds to introducing a branch point *without changing the energy density*. These sequences therefore describe the local structure at bifurcations that introduce branch points in energy minimizers.

Recursively replicating the above process introduces multiple branch points on the surface, as illustrated in fig. 2. We start with $w(x, y) = xy$ and introduce a branch point $b_{1,1} = (1/\sqrt{2}, 1/\sqrt{2})$ with the angle sequence $\{0, \frac{\pi}{6}, \frac{\pi}{3}, \frac{\pi}{2}, \pi, \frac{3\pi}{2}, 2\pi\}$; see fig. 2(a). Three more branch points $b_{2,1}, b_{2,2}, b_{2,3}$ can be added, one within each new sector, by introducing lines of inflection at angles $\{\frac{\pi}{18}, \frac{\pi}{9}, \frac{2\pi}{9}, \frac{5\pi}{18}\}$ and $\{\frac{7\pi}{18}, \frac{4\pi}{9}\}$ respectively; see Fig 2(b). The solution can be extended by odd periodic reflections about the x and y axes to give a small-slope isometric immersion of \mathbb{R}^2 with $K = -1$; see fig. 2(c). The branch points $b_{1,1}, b_{2,1}, b_{2,2}$ and $b_{2,3}$ are 3-saddles, *i.e. monkey saddles*. The resulting surface is not smooth, but it has a Lipschitz continuous tangent plane, bounded principal curvatures and finite

bending energy density. It also displays *sub-wrinkling* or *refinement* – the “number of waves” increases with r . Our construction illustrates the key role of branch points in circumventing the rigidity (eq. (5)) of smooth solutions of (3).

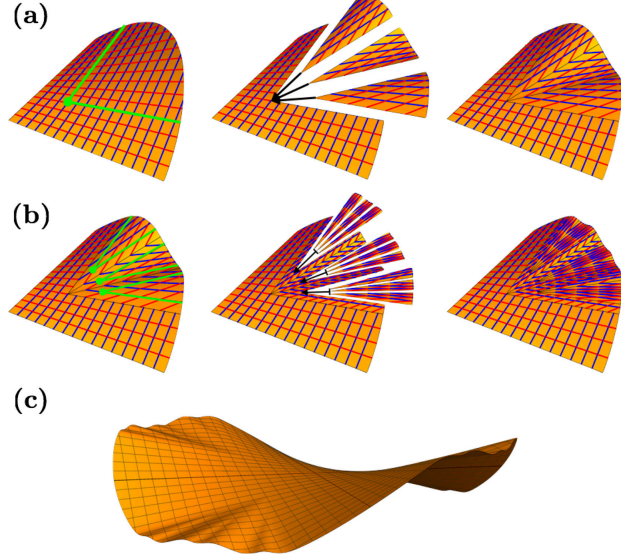


Fig. 2: Solutions to $\det(D^2w) = -1$ with branch points. (a) Three sub-wrinkle solution on the first quadrant. (b) Nine sub-wrinkle solution. (c) Extension to 36 sub-wrinkle solution on the plane.

We now return to the strip geometry in eq. (2); we want to create patterns which have an effective wavelength that increases with y , so they have lower energy than the single wavelength isometry. A natural idea is to introduce branch points into the product solutions of eq. (3) to allow for local refinement of the wavelength near $y = 0$. However, the product solutions are not ruled by straight lines, and it is not immediately obvious how one adapts the above construction.

We can construct solutions of eq. (3) as follows. Let $Z(X, Y)$ be a (piece of a) surface satisfying $Z_{XX}Z_{YY} - (Z_{XY})^2 = -1$ with $Z_{XX} \neq 0, Z_{YY} \neq 0$ (true generically by rotating the XY -axes if necessary). Define $P = \partial_X Z, Q = \partial_Y Z, \sigma = (f''(y))^{1/4}$. Direct computation shows that the over-determined system

$$\begin{aligned} \partial_Y y &= -\sigma^{-2}, & x &= \sigma^{-1} (X + \xi_+ + \xi_-), \\ \partial_x w &= P, & \partial_y w &= \sigma (Q + \xi_+ - \xi_-), \end{aligned} \quad (6)$$

satisfies $\partial_y(\partial_x w) = \partial_x(\partial_y w), \det(D^2w) = -f''(y)$ if and only if

$$\frac{\partial \xi_{\pm}}{\partial Y} \mp \frac{\partial \xi_{\pm}}{\partial P} = \frac{\partial_Y \sigma}{2\sigma} (X \mp Q + 2\xi_{\mp}) \text{ and } \det(D^2Z) = -1. \quad (7)$$

Solving eq. (7) reduces to integrating ODEs on surfaces satisfying $\det(D^2Z) = -1$. If the underlying surface $Z(X, Y)$ has branch points, then so does the surface $w(x, y)$. Consequently there exist many non-smooth solutions to (3) for metrics with y -dependent growth. In particular eq. (6) yields $(1 + y/l) \sim Y^{-2}$ for the metric in ref. [2]; in this case and refinement with increasing Y for $Z(X, Y)$ corresponds to sub-wrinkling as $y \rightarrow 0$.

Instead of using Eqs. (6)-(7), we directly generate discrete *Asymptotic nets* [30] (allowing for potential branch points) that solve (a discretization of) eq. (3) – it is easier to impose boundary conditions in the latter approach. Figure 3(a) illustrates a “discrete isometric immersion” obtained by introducing branch points into the product solution of eq. (3). As the step size of the discretization goes to zero, the asymptotic net converges, by construction, to a surface with a continuously varying tangent plane, *i.e.* no ridges or cone-points. As expected from eqs. (6)-(7), our numerical algorithm generates a quad-mesh with the same topology as the meshes in fig. 2(b). Figure 3(b) demonstrates the convergence of the asymptotic net to an isometry of the metric in (2) with $\alpha = 1$ by comparing the (nondimensional) “target curvature” $K(y) = -f''(y)$ with the piecewise constant discrete Gaussian curvature K_d of the asymptotic net.

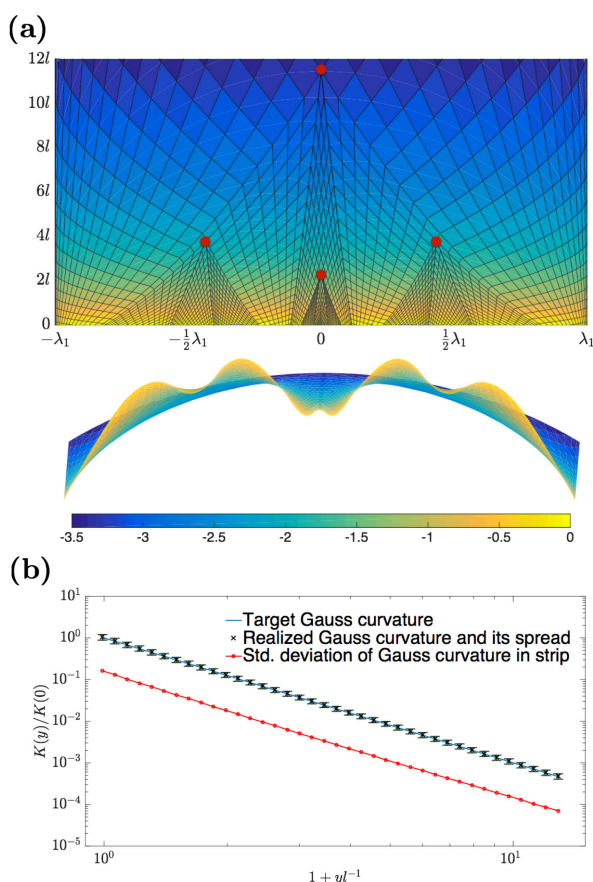


Fig. 3: (a) Discrete approximation of a four branch point (highlighted) isometric immersion for growth profile $f(y) \sim (1 + y/l)^{-1}$. The surface is colored by $\log_{10}(K_d/K(0))$, the logarithm of the discrete curvature; note that the curvature (essentially) only depends on y . (b) Mean and spread of the discrete Gaussian curvature on thin “horizontal” strips.

Given a solution $w(x, y)$ of eq. (3) we obtain a 2-parameter family of rescaled solutions by $\tilde{w}(x, y) = s_1^{-2} s_2^2 w(s_1 x, s_2(y + l) - l)$, with scale factors $s_1 > 0$, $s_2 \geq 1$. Figure 4(a) shows the minimum energy among isometries obtained by rescaling the solution shown in fig. 3. As W/l increases, it is indeed energetically favorable to introduce branch points in $0 \leq y \leq W$; fig. 4(b) il-

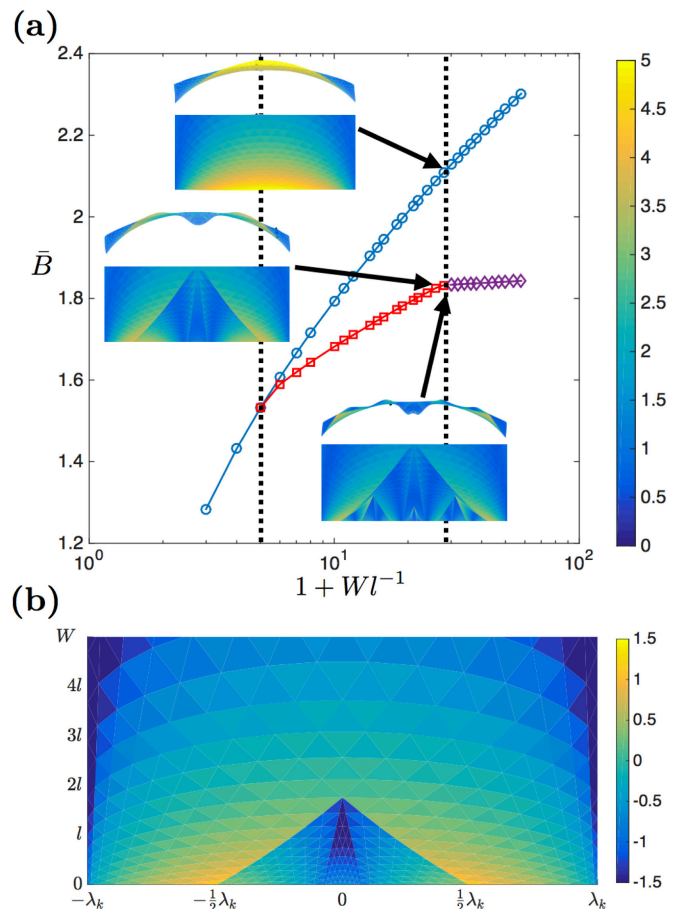


Fig. 4: (a) Bending energy minimized over a 2-parameter family of isometries for $\alpha = 1$. Circles (blue) correspond to single wavelength isometries, squares (red) to surfaces with one branch point, diamonds (magenta) to surfaces with three or four branch points. Inset surfaces are colored by the nondimensional energy density $l^2(\kappa_1^2 + \kappa_2^2)$. (b) The disparity η for the energy minimizing solution with $1 + Wl^{-1} = 6$. This figure is to scale. The optimal values are $s_1 \approx 9.1$, $s_2 \approx 4.9$, $\lambda_k \approx 5.1l$.

lustrates that the first branch point appears when $\eta \approx 1$ at $(0, 0)$. The insets in fig. 4(a) illustrate the divergence of H with increasing W/l for single wavelength isometries; they also show that introducing branch points does lower the bending energy.

Exponential metrics and singular edges. – As a special case we now consider the metric:

$$\mathbf{g} = (1 + \epsilon^2 \exp(-2y/l))dx^2 + dy^2 \quad (8)$$

on the half-plane $\mathbb{R}_+^2 = \mathbb{R} \times [0, \infty)$, and also on all of \mathbb{R}^2 . Equation (3) has a one parameter family of solutions on \mathbb{R}^2 :

$$w^0(x, y) = \sqrt{2}k^{-1} \cos(kx) \exp(-y/l).$$

For $k = l^{-1}$, $w^0(x, y)$ is a harmonic function on \mathbb{R}^2 and $H = 0$ (a minimal surface) in the small-slope approximation. Consequently, there is no mechanism in the small-slope regime to drive sub-wrinkling. The metric (8) thus provides a natural setting to isolate/study nonlinear effects in exact (*i.e.* non small-slope) isometries on wrinkling patterns in hyperbolic sheets.

We can find analytic isometries of the metric by power series expansions: $(x, y) \mapsto (x + \epsilon^2 u, y + \epsilon^2 v, \epsilon w)$ where $u = \sum_{i=0}^{n-1} \epsilon^{2i} u^i$, $v = \sum_{i=0}^{n-1} \epsilon^{2i} v^i$ and $w = \sum_{i=0}^{n-1} \epsilon^{2i} w^i$ and w^0 is as above. In terms of the Airy bracket $[h, g] = \frac{1}{2} (h_{xx} g_{yy} - 2h_{xy} g_{xy} + h_{yy} g_{xx})$ [27], the solvability conditions for zero in-plane strains at $O(\epsilon^{2n+2})$, and the corresponding solutions w^n are given by:

$$0 = \sum_{i=0}^{n-1} \left([u^i, u^{n-i-1}] + [v^i, v^{n-i-1}] \right) + \sum_{i=0}^n [w^i, w^{n-i}],$$

$$w^n(x, y) = k^{-1} e^{-(2n+1)y/l} \sum_{i=0}^n a_{i,n} \left((kl)^{-1} \right) \cos((2i+1)kx),$$

where $n \geq 1$ and $a_{i,n}$ are polynomials. Convergent power series $\sum_{i=0}^{\infty} \epsilon^{2i} w^i : \mathbb{R}_+^2 \rightarrow \mathbb{R}$ yield analytic isometric immersions of the half-plane \mathbb{R}_+^2 with metric (8) into \mathbb{R}^3 .

We can access the non small-slope regime by increasing ϵ . In eq. (8) this is equivalent to keeping ϵ fixed, say $\epsilon = 1$ and shifting y . For sufficiently small ϵ , the power series for w, u and v converge on \mathbb{R}_+^2 , so the power series with $\epsilon = 1$ converges on $\mathbb{R}_+^2 + (0, \lambda_0)$ for some shift λ_0 . Increasing ϵ is equivalent to shifting the domain in the negative- y direction, *i.e.*, extending the domain of the isometric immersion with $\epsilon = 1$. Efimov's theorem [19] thus implies, for any smooth isometric immersion of \mathbb{R}_+^2 , a principal curvature will diverge with increasing ϵ . Amster's theorem [18] suggests that for any $\epsilon > 0$, the isometries will develop a *singular edge* in \mathbb{R}^2 corresponding to the boundary of the domain where the power series converges.

With increasing ϵ , the singular edge will first intersect with the half-plane \mathbb{R}_+^2 at $(0, 0)$, *i.e.* where $|\partial_{yy}^2 w|$ attains its maximum. If $\partial_{yy}^2 w(0, y) \sim A(y + \epsilon - \epsilon_0)^{-(\beta+1)}$, we can approximate ϵ_0 and β by the poles and residues of the Padé approximants to the logarithmic derivative $\partial_{yy}^2 w(0, 0)/\partial_y w(0, 0)$ [31]. In fig. 5 we plot the Dlog Padé approximants for the case $kl = 1$ and find that $\epsilon_0 \approx 2.86$ and $\beta = .500158$. This strongly indicates that a curvature diverges as $s^{-\frac{1}{2}}$, where s is the distance to the singular edge. This divergence is consistent with the singular edge of the pseudosphere and other hyperbolic surfaces of revolution.

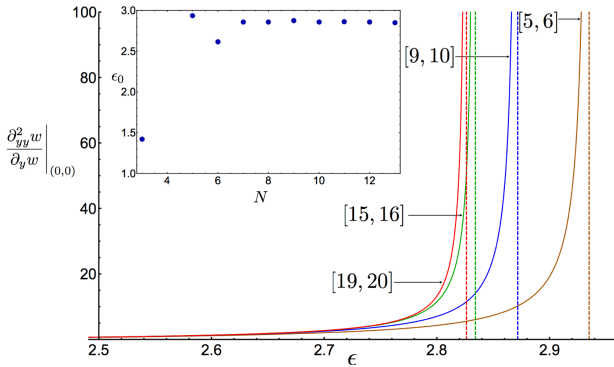


Fig. 5: $[N, N + 1]$ Padé approximants to the logarithmic derivative $\partial_{yy}^2 w/\partial_y w$ at $(0, 0)$. The inset figure is a plot of the value(s) of ϵ_0 inferred from the vertical asymptote of the $[N, N + 1]$ Padé approximants.

The divergence of a principal curvature has consequences for modeling non-Euclidean elastic sheets. In particular, as ϵ gets

larger, the minimizers of the small-slope approximation may not capture the behavior of the minimizers of the full elastic energy *even qualitatively*. Figure 6 shows a contour plot of $\overline{\mathcal{B}}[\Delta w] = l^{-1} \lambda_k^{-1} \int_0^{\lambda_k} \int_0^{\infty} (\Delta w)^2 dy dx$ computed from the [9, 9] Padé approximant of Δw . The solid line indicates the ϵ dependent global wavelength $\lambda_{glob} \sim k^{-1}$ that minimizes $\overline{\mathcal{B}}$, a proxy for the bending energy per unit length. For $\epsilon \ll 1$ the full elastic energy selects the expected wavelength from the small slope theory, *i.e.* $k = l^{-1}$, while for moderate values of $\epsilon \gtrsim 2$ the singular edge has a dramatic influence on the bending energy.

The sheet can “move” the singular edge by a global decrease of the wavelength, *i.e.* making k larger. While this lowers the bending content near $y = 0$, it will introduce large bending content in the rest of the sheet. As in the small-slope case, we expect that the minimizers of the elastic energy will instead locally refine the wavelength by introducing branch points near the edge $y = 0$. The first branch point is expected to occur on the dash-dotted line in fig. 6 corresponding to the contour $H/\sqrt{|K|} = \eta = 1$. The sub-wrinkling threshold for energy minimizers is at the intersection of the curves, *i.e.*, $\epsilon \approx 1.75$. Accounting for in-plane displacement, this corresponds to a slope $\gamma = |\partial_y w|/\sqrt{1 - (\partial_y w)^2} \approx 0.67$. Complex buckling patterns can thus occur even in situations where the small-slope theory would predict no sub-wrinkling. Nonlinear contributions to in-plane strains are relevant for slopes as small as $\tan^{-1}(\gamma) \approx 35^\circ$; this is consistent with the “real world” examples in fig. 1.

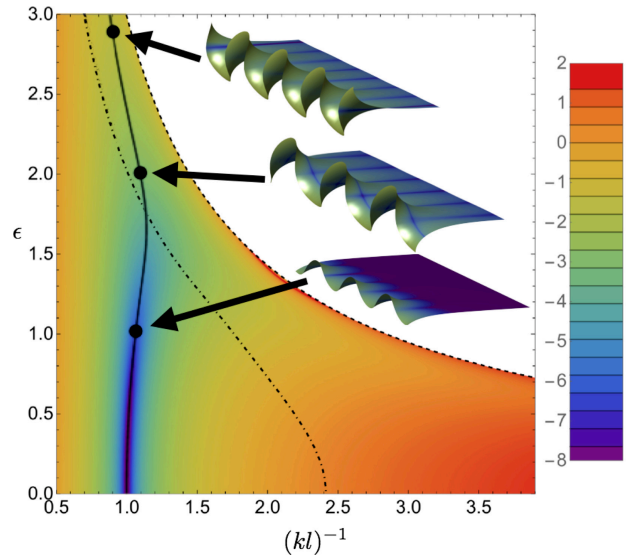


Fig. 6: Contour plot of $\ln(\overline{\mathcal{B}})$ as a function of the dimensionless wavelength $(kl)^{-1}$ and ϵ . $\eta = 1$ on the dash-dotted line and the solid line is the energy minimizing wavelength. The dashed curve indicates values at which the singular curve touches $(0, 0)$; it represents a “horizon” *i.e.* a limit to the extension of an isometry.

Discussion. – The existence of small-slope isometric immersions for hyperbolic free sheets with finite bending content ensures that the elastic energy per unit thickness scales as t^2 . This is much smaller than $t^{5/3}$, the energy scale for crumpled sheets [25, 32] as $t \rightarrow 0$. Free sheets do not have elastic

ridges [25] or d -cones [26]; rather, the relevant singularities are *branch points* and *lines of inflection*. These defects are unique in that they *do not concentrate elastic energy* in the vanishing thickness limit. They arise for geometric reasons, *viz.* to bypass the rigidity of smooth isometric immersions (eq. (5)) that prevents the refinement of the pattern wavelength. To our knowledge, this is the first example of a condensed matter system that is driven by *geometric* rather than *energetic* defects.

We have shown that the buckling patterns in free sheets are a result of competition between the contributions to the bending energy from the two principal curvatures, and not, as was previously believed, from a competition between stretching and bending. Our key contribution is in identifying a mechanism, *viz.* the introduction of branch points/lines of inflection, that lowers the bending energy of the sheet while preserving the isometry constraint and the Lipschitz continuity of the tangent plane. We analyze this mechanism and give a quantitative criterion for incipient sub-wrinkling in free sheets. Additionally, the nonlinear contributions to the strain from the in-plane displacements can drive multiple-scale buckling and generate branch points in free elastic sheets. For wide ($W/l \gtrsim O(1)$) hyperbolic elastic sheets, one expects, generically, to find branch points and lines of inflection since fractal-like, sub-wrinkling, profiles have lower energies than their single wavelength counterparts.

This work is primarily concerned with the vanishing thickness limit $t \rightarrow 0$. The results however are immediately transferable to physical sheets. In a physical sheet, the lines of inflection and branch points are replaced by boundary layers; the sheet configuration is indeed smooth, albeit with small scale structures. We expect that the smoothed defects are akin to the $t^{1/3}$ and $t^{1/2}$ boundary layers that resolve the non-smoothness of the n -saddle isometries of disks with $K = -1$ [33].

Our construction shows there are *continuous families* of low-energy states obtained by appropriately gluing together isometries, and “floppy modes” that come from variations within these families. Consequently, thin hyperbolic free sheets are easily deformed by weak stresses and the pattern selected may be sensitive to the dynamics of the swelling process, experimental imperfections, or other external forces. A statistical description of the singularities and their interactions is therefore a natural approach to study this system, in contrast to a static approach that seeks to find the global energy minimum. This problem is indeed very much open; a first step might be to analyze the energy scaling of a surface with a prescribed distribution of branch points. This is challenging analytically – there are various relevant length scales: $\sqrt{|K|}$, W , l and scales in the distribution of the defects, and also numerically – we need methods that discretize potentially non-smooth solutions while ensuring appropriate continuity of the tangent plane.

* * *

JG, ES and SV were supported in part by an US-Israel BSF grant 2008432. JG and SV were also supported in part by the NSF grant DMS-0807501. JG is currently supported by NSF-RTG grant DMS-1148284. This research was supported in part by the NSF through Grant No. NSF PHY11-25915.

REFERENCES

- [1] SHARON E., ROMAN B., MARDER M., SHIN G.-S. and SWINNEY H. L., *Nature*, **419** (2002) 579.
- [2] AUDOLY B. and BOUDAOU A., *Phys. Rev. Lett.*, **91** (2003) 086105.
- [3] SHARON E., ROMAN B. and SWINNEY H. L., *Phys. Rev. E*, **75** (2007) 046211.
- [4] AUDOLY B. and BOUDAOU A., *Comptes Rendus Mecanique*, **330** (2002) 831.
- [5] MARDER M., SHARON E., SMITH S. and ROMAN B., *Europhys. Lett.*, **62** (2003) 498.
- [6] MARDER M., *Foundations of Physics*, **33** (2003) 1743.
- [7] MARDER M. and PAPANICOLAOU N., *J. Stat. Phys.*, **125** (2006) 1065.
- [8] LIANG H. and MAHADEVAN L., *Proc. Nat. Acad. Sci.*, **106** (2009) 22049.
- [9] EFRATI E., KLEIN Y., AHARONI H. and SHARON E., *Physica D: Non-linear Phenomena*, **235** (2007) 29.
- [10] KLEIN Y., EFRATI E. and SHARON E., *Science*, **315** (2007) 1116.
- [11] KIM J., HANNA J. A., BYUN M., SANTANGELO C. D. and HAYWARD R. C., *Science*, **335** (2012) 1201.
- [12] GORIELY A. and AMAR M. B., *Phys. Rev. Lett.*, **94** (2005) 198103.
- [13] BEN AMAR M. and GORIELY A., *J. Mech. Phys. Solids*, **53** (2005) 2284.
- [14] ORTIZ M. and GIOIA G., *J. Mech. Phys. Solids*, **42** (1994) 531.
- [15] BEN BELGACEM H., CONTI S., DESIMONE A. and MÜLLER S., *J. Nonlinear Sci.*, **10** (2000) 661.
- [16] BELLA P. and KOHN R. V., *J. Nonlinear Sci.*, **24** (2014) 1147.
- [17] HAN Q. and HONG J.-X., *Isometric embedding of Riemannian manifolds in Euclidean spaces* (AMS, Providence, RI) 2006.
- [18] AMSLER M.-H., *Mathematische Annalen*, **130** (1955) 234.
- [19] EFIMOV N. V., *Matematicheskii Sbornik*, **106** (1964) 286.
- [20] NECHAEV S. and VOITURIEZ R., *J. Phys. A: Mathematical and General*, **34** (2001) 11069.
- [21] EFRATI E., SHARON E. and KUPFERMAN R., *J. Mech. Phys. Solids*, **57** (2009) 762.
- [22] FUNG Y. C., *Foundations of solid mechanics* (Prentice-Hall, Englewood Cliffs, N.J.) 1965.
- [23] LEWICKA M., MAHADEVAN L. and PAKZAD M. R., *Proc. Roy. Soc. London Ser. A*, **467** (2011) 402.
- [24] LEWICKA M. and REZA PAKZAD M., *ESAIM: Control, Optimisation and Calculus of Variations*, **17** (2011) 1158.
- [25] LOBKOVSKY A. E., *Phys. Rev. E*, **53** (1996) 3750.
- [26] BEN AMAR M. and POMEAU Y., *Proc. Roy. Soc. London Ser. A*, **453** (1997) 729.
- [27] AUDOLY B. and POMEAU Y., *Elasticity and geometry: from hair curls to the non-linear response of shells* (Oxford University Press Oxford) 2010.
- [28] GEMMER J. A. and VENKATARAMANI S. C., *Physica D: Nonlinear Phenomena*, **240** (2011) 1536.
- [29] RUDIN W., *Principles of mathematical analysis* Vol. 3 (McGraw-Hill New York) 1964.
- [30] BOBENKO A. I. and PINKALL U., *Oxford lecture series in mathematics and its applications*, **16** (1999) 3.
- [31] BAKER JR G. A., *Physical Review*, **124** (1961) 768.
- [32] LOBKOVSKY A., GENTGES S., LI H., MORSE D. and WITTEN T. A., *Science*, **270** (1995) 1482.
- [33] GEMMER J. and VENKATARAMANI S., *Nonlinearity*, **25** (2012) 3553.